



universität
wien

BACHELORARBEIT / BACHELOR'S THESIS

Titel der Bachelorarbeit / Title of the Bachelor's Thesis

„Simulation and optimisation of microstrip antennas for
propagating spin-wave spectroscopy“

verfasst von / submitted by

Fabian Alexander Polnitzky

angestrebter akademischer Grad / in partial fulfilment of the requirements for the degree of
Bachelor of Science (BSc)

Wien, 2023 / Vienna, 2023

Studienkennzahl lt. Studienblatt /
degree programme code as it appears on
the student record sheet:

UA 033 676

Studienrichtung lt. Studienblatt /
degree programme as it appears on
the student record sheet:

Bachelor Physics

Betreut von / Supervisor:

Univ.-Prof. Dr. habil. Andrii Chumak

Abstract

The research area concerning itself with the data procession using spin waves is called magnonics and the quanta of one spin wave is the magnon [18]. Microstrip antennas can be used to excite and detect electromagnetic waves. They can also be used to induce and record a spin wave in specific materials. However optimal microstrip antennas are needed and it has to be known which properties can influence the propagation. This characterization of three sets of microstrip antennas and the investigation of the electromagnetic leakage between the antennas are the goals of this thesis. Both experimental and numerical tools were employed for this. In the experiment the transmission of the antennas was recorded using a vector network analyzer and the measurements were done in different settings to analyze multiple effects. The numerical results were obtained by simulation where one of the experiments was recreated. For both the transmission was characterized using the scattering parameters. The structures under investigation were three sets of microstrip antennas all with a different distance between the antennas. Additionally the one with the largest distance has a capacitor-like ground while the others have real direct grounds. The set with the smallest distance was measured in multiple different geometries for comparison and no influence on the general transmission was observed. The other two sets were measured in only one geometry and the sets were compared among each other. For larger distances between the antennas the measurement results showed more features and noise. Also an experiment using a Yittrium Iron garnet waveguide to excite a spin wave was carried out for all sets. The signal of this wave was observed, however it appeared at different frequencies for the smallest distance and the other sets which should not be the case and no clear explanation for this was found. The simulation was performed for the two sets with real direct ground and the results were compared to the experimental ones. No strong deviation were observed. However the numerical results displayed a series of peaks which are possibly associated with the formation of standing electromagnetic waves in the antennas. Length scales corresponding to the waves were calculated and an attempt at assigning them to lengths in the simulation model was made. Additionally some peaks in the experimental results were present, but it can be shown that these can be removed and did not change the general statement.

Contents

Abstract	i
List of Tables	v
List of Figures	vii
1 Introduction	1
2 Theoretical background	5
2.1 Maxwell's equations	5
2.2 Landau-Lifshitz-Gilbert equation	6
2.3 Characteristic impedance	7
2.4 Skin effect	9
2.5 Microstrip lines	9
3 Setup, material and methods	11
3.1 Experimental setup and methods	11
3.1.1 The experimental setup	11
3.1.2 Vector network analyzer and scattering parameters	11
3.1.3 Measurements	13
3.2 COMSOL Multiphysics	14
4 Results	19
4.1 Experimental results	19
4.1.1 4 mm distance set of microstrip antennas in different geometries . .	19
4.1.2 Comparison of the results for the structures under investigation . .	21
4.2 Comparison of the simulation and the experimental results	23
5 Discussion	29
5.1 4 mm distance set of microstrip antennas in different geometries	29
5.2 Comparison of the results for the structures under investigation	31
5.3 Comparison of the simulation and the experimental results	33
6 Conclusion	35
Bibliography	37

List of Tables

3.1	The dimensions of the model in COMSOL for the 10 mm distance set of microstrip antenna. The first column gives a name and the third a description of the length stated. The second column gives the value in mm or in mil if stated.	15
3.2	The material properties for the two materials used.	15
4.1	The peaks for the 4 mm distance set of microstrip antennas for both Study 1 and Study 2.	25
4.2	The peaks for the 10 mm distance set of microstrip antennas for both Study 1 and Study 2.	25

List of Figures

1.1	A picture of the 13-channel MSW filterbank device and the graph showing the measurements of the transmission loss (Both graphs taken from [2]).	2
2.1	The phenomenon described by the LLG equation can be seen here. In (a) the precession of the magnetization m around the effective field H^{eff} is shown. In (b) the motion of m towards the effective field can be seen. In (c) both parts are added to give the spiral motion of the magnetization around H^{eff} (Graph taken from [1]).	7
2.2	A lumped-element circuit as a model for a transmission line of length Δz (Graph taken from [16]).	8
2.3	The schematic drawing of a microstrip line. In (a) the design is shown and important lengths and constants are indicated. The grey area is the dielectric substrate. In (b) this is viewed from the front. The electric field as black lines and the magnetic field as dashed lines are depicted here (Graph taken from [16]).	10
3.1	The experimental setup is shown here. On the left is the VNA already displaying a measurement and on the right is the electromagnet with a set of microstrip antennas between the poles. The two are connected by coaxial cables.	12
3.2	Two of the sets of microstrip antennas. On top a technical design of the set of microstrip antennas is shown and on the bottom an image of one with holder, end-launch connectors and screws of the coaxial cables can be seen.	13
3.3	A picture of the three dimensional model from COMSOL for the 10 mm distance set of microstrip antennas.	16
4.1	Measurements of the 4 mm distance set of microstrip antennas outside the magnet in blue and inside the magnet without an external field in orange. The title of the plot indicates the measured geometry. The frequency in GHz is given on the x-axis and S_{21} in dB on the y-axis.	19
4.2	Measurements of the 4 mm distance set of microstrip antennas inside the magnet with two different field strengths in blue and orange and for the surface geometry in magenta as the field strength is different here (see legend of the plots for the values). The title of the plot indicates the measured geometry. The frequency in GHz is given on the x-axis and S_{21} in dB on the y-axis. Here no YIG waveguide is present.	20

List of Figures

4.3	Measurements of the 4 mm distance set of microstrip antennas inside an external field of 350 mT with the YIG waveguide on top of it in orange and without in blue. Here the x-axis is the same as before, but only a part of the spectrum is shown, and the y-axis in dB shows the S_{12} parameter.	20
4.4	Measurements of the three sets of microstrip antennas outside in blue and inside the electromagnet without an external field in orange. The different distances between the single antennas is given in the title of the plots. The frequency in GHz is given on the x-axis and S_{21} on the y-axis in dB.	22
4.5	Measurements of the three sets of microstrip antennas inside the magnet with two different field strengths in blue and orange and for the largest distance between the antennas on the right in magenta as the field strength is different here (see legend of the plots for the values). The y-axis shows the S_{21} parameter in dB, the x-axis the frequency in GHz and the titles indicate the distance of the used set of antennas. Here no YIG waveguide is present.	23
4.6	Measurements of the three sets of microstrip antennas inside an external field of 350 mT with the YIG waveguide on top of it in orange and without in blue. The x- and y-axis are the same as before and the title states the distance of the measured set of antennas. However the frequency range is different for the left plot from the rest, the middle and right one have the same range.	24
4.7	The results for the experiment and the simulation for the 4 mm distance set of microstrip antennas. In black the experimental result, in blue the results for Study 1 and in orange for Study 2 can be seen. The x-axis displays the frequency in GHz and on the left the y-axis shows the S_{11} and on the right the S_{21} parameter, both in dB.	25
4.8	The results for the experiment and the simulation for the 10 mm distance set of microstrip antennas. In black the experimental result, in blue the results for Study 1 and in orange for Study 2 can be seen. The x-axis displays the frequency in GHz and on the left the y-axis shows the S_{11} and on the right the S_{21} parameter, both in dB.	26
4.9	The results for the S_{21} parameter for both sets of microstrip antennas and both studies. The title of the single plots states which set of microstrip antennas and study is shown. The blue graph is the simulation result and the black dots indicate the found peaks. The legend in the lower right plot is valid for all of them. The x-axis displays the frequency in GHz and the y-axis S_{21} in dB.	27
5.1	The smoothed experimental results of the measurements of the 4 mm distance set of microstrip antennas in the forward volume geometry. For axis and color descriptions see figure 4.1. The settings of the filter are given in the title of the plot. Here just a part of the y-axis range is shown.	30

- 5.2 The smoothed experimental results of the measurements of the 4 mm distance set of microstrip antennas in backward volume geometry. For axis and color descriptions see figure 4.2. The settings of the filter are given in the title of the plot. Here just a part of the y-axis range is shown. 31

1 Introduction

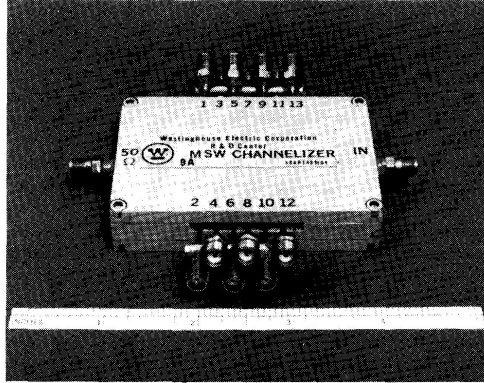
The research on radio frequency and microwave devices has been going on for quite some time now with the first one being the cat-whisker crystal detector in the nineteenth century. During the interwar period experiments on waveguides were conducted and frequency conversion and heterodyning arose. In the 1960s devices utilizing microwaves semiconductors were researched and developed. In present time radio frequency and microwave devices can be found nearly everywhere in the daily life. In smartphones, WiFi, satellites for radio and television broadcast, global positioning system to just name a few examples [16].

In the 1970s Adam et al. measured the ferromagnetic linewidth in Yttrium Iron garnet (YIG) grown on Gadolinium Gallium garnet (GGG). This was done to determine its microwave performance and it was concluded that YIG can be used for specific applications for microwave communication filters [3]. Some years later J. D. Adam presented in a review a 13-channel filterbank. Each channel corresponds to one delay line made of YIG on GGG. For the propagation of magnetostatic waves (MSW) a magnetic field was oriented perpendicular and out of plane of the YIG waveguide. The different channels were achieved because the magnetic field was not constant in space, so each YIG waveguide had different MSWs. In figure 1.1 the 13-channel filterbank can be seen and below the measurement of the transmission loss in dB on the y-axis and the frequency in GHz on the x-axis. It can be verified in the graph that the channels are evenly distributed and the out-of-band rejection at 75 dB can be seen. Other devices like a frequency selective limiter are also presented. For the two devices it is shown that they could have competed with system requirements during the time [2]. Seven years later in 1995 a number of filters using magnetostatic surface spin waves (MSSW) were presented, namely frequency-selective fixed-tuned filters, nonlinear filters, tunable and channel filters [13].

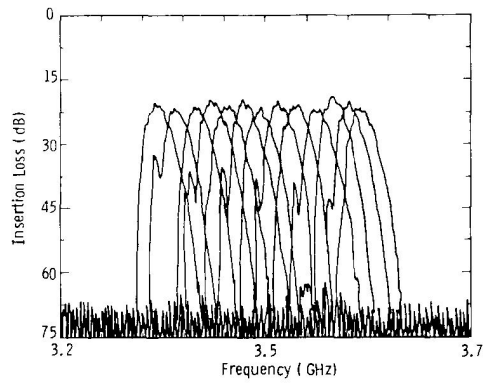
In this century the focus of the research area shifted a bit to the use of spin waves to transport information and the field received a new name, magnonics [18]. The quantized spin waves are referred to as magnons. Advantages are among others the improved data processing and scalability of the devices utilizing spin waves. One important property is also the frequency range in which the devices can be operated, from a few GHz even up to a few hundred THz [4].

In general the purpose of a filter is to dismiss certain parts of the frequency spectrum and to conserve another part. A band pass filter has two specific frequencies and lets frequencies between these two values pass and removes the outside values [15]. For a band pass filter the center frequency is defined as the arithmetic or geometric mean of the two specific frequency values. The width of the band pass filter is referred to as the bandwidth. The out-of-band rejection describes the ability to attenuate signals that

1 Introduction



(a) The device with magnet.



(b) The transmission loss with frequency in GHz on the x-axis and insertion loss in dB on the y-axis.

Figure 1.1: A picture of the 13-channel MSW filterbank device and the graph showing the measurements of the transmission loss (Both graphs taken from [2]).

could interfere, but are further away from the band. The insertion loss describes the ratio of a signal without and with a filter [14].

When inputting a current in an antenna an alternating magnetic field is generated. The field then interacts with the magnetic waveguide present and causes a spin wave to propagate. The detection of this wave at a second antenna then works the opposite way [18]. For MSWs travelling in epitaxial grown YIG the magnetic bias field determines the center frequency and the bandwidth depends on the saturation magnetization [2]. The width of the antenna is a lower limit for the spin wave wavelength. Losses are caused by the efficiency of exciting and detecting a spin wave and the waves dissipation in the waveguide. The transmission signal outside of the frequency of the spin wave is due to electromagnetic leakage between the antennas [18] which means this is also responsible for the out-of-band rejection.

This thesis aims to analyze the performance of microstrip antennas and to investigate the electromagnetic leakage between them using multiple types and different methodologies. The structures under investigation are two sets of microstrip antennas with real direct ground using a via and two different distances between the antennas and one set with capacitor-like ground and different distance. The measurement aims to characterize electromagnetic waves passing between the two microstrip antennas of one set. The first set of microstrip antennas is measured without a magnetic field outside and inside an electromagnet to determine the influence of the metallic poles on the wave transmission. This is done in three different geometries in the magnet. Additionally measurements of the electromagnetic leakage in a magnetic field and of spin wave propagation in the geometries are carried out and the measurement results are compared against each other. For the other two microstrip antennas the measurements are also done, but in only one geometry and the results will be compared among the sets. Additionally to the experiments simulations are performed for the two sets of microstrip antennas with real direct ground, again with the same goal. The results will then be compared with the respective measurement results.

The next chapter will present the theoretical background which this work deals with. Maxwell's equations and the Landau-Lifshitz-Gilbert (LLG) equation is motivated. A derivation of the characteristic impedance is given. The skin effect and microstrip lines are explained afterwards. Next the methodology is presented. The experimental setup is explained and concepts important for the measurements are described. The simulation and the workflow of it is introduced. After that the obtained results will be presented, first the experimental and then the numerical, and in the next chapter discussed. Lastly a summary and conclusion of this work is given.

2 Theoretical background

In this chapter the theoretical background used to describe the phenomena which are explored further are introduced. First Maxwell's equations for electric and magnetic fields are shown, for vacuum and with a material present. Next the equation describing the change in time of the magnetization, the Landau-Lifshitz-Gilbert (LLG) equation is motivated. After that the characteristic impedance is derived and the skin effect is introduced. Lastly the basics of microstrip lines are described.

2.1 Maxwell's equations

The relation between an electric field \vec{E} and the magnetic induction \vec{B} is given by Maxwell's equations. These are a set of coupled differential equations. The first two describe both fields independently.

$$\nabla \cdot \vec{E} = \frac{\rho}{\epsilon_0} \quad (2.1)$$

$$\nabla \cdot \vec{B} = 0 \quad (2.2)$$

Here ∇ is the Nabla operator which is defined in three dimensions as $\nabla = \frac{\partial}{\partial x}\hat{x} + \frac{\partial}{\partial y}\hat{y} + \frac{\partial}{\partial z}\hat{z}$ with \hat{x} , \hat{y} , \hat{z} being the unit vectors in three dimensions. ρ here means the charge density and ϵ_0 is the permittivity. Equation 2.1 comes from Coulomb's law. The Nabla operator gives the spatial change of the electric field and the equation says the lines of an electric field go from a positive charge to a negative. Equation 2.2 states that the lines of a magnetic field are only present in curves with no start or end, but are closed.

The last two equations describe how the two fields influence each other.

$$\nabla \times \vec{E} = -\frac{\partial \vec{B}}{\partial t} \quad (2.3)$$

$$\nabla \times \vec{B} = \mu_0 \vec{J} + \mu_0 \epsilon_0 \frac{\partial \vec{E}}{\partial t} \quad (2.4)$$

Equation 2.3 is also described by Faraday's law of electromagnetic induction. On the left hand side of both equations the curl, the cross product with the fields is calculated. The operation describes the circulation of a field. Here the circulating electric field is given around a magnetic induction changing in time. Equation 2.4 for a stationary electric field ($\partial \vec{E} / \partial t = 0$) is similar to Ampere's law which says that an electric current with current density \vec{J} generates a magnetic field around it. μ_0 here is the permeability of free space.

2 Theoretical background

If now there is matter present some variables in the equations above change. The current density can be separated into the current \vec{J}_{free} and the currents \vec{J}_{bound} which are caused by the circular motion of the electrons around the nucleus. The overall current density is then the sum of the two.

$$\vec{J} = \vec{J}_{free} + \vec{J}_{bound} \quad (2.5)$$

The currents caused by the electrons also have an influence on the magnetization \vec{M} , in case of an electric field not changing with time with

$$\nabla \times \vec{M} = \vec{J}_{bound} \quad (2.6)$$

and similar to this

$$\nabla \times \vec{H} = \vec{J}_{free} \quad (2.7)$$

with the magnetic field \vec{H} . The relation between the magnetic field, induction and magnetization is

$$\vec{B} = \mu_0 (\vec{H} + \vec{M}) \quad (2.8)$$

With this relation equation 2.2 can be rewritten with substituting \vec{B} in the equation by \vec{H} and \vec{M} which gives

$$\nabla \cdot \vec{H} = -\nabla \cdot \vec{M} \quad (2.9)$$

which means the magnetic field itself does have sources.

If a material is present it can have an electric polarization \vec{P} which is related to the electric field with

$$\vec{D} = \epsilon_0 \vec{E} + \vec{P} \quad (2.10)$$

where \vec{D} is the electric displacement. With all the additional quantities Maxwell's equations can be written in

$$\nabla \cdot \vec{D} = \rho_{free} \quad (2.11)$$

$$\nabla \cdot \vec{B} = 0 \quad (2.12)$$

$$\nabla \times \vec{E} = -\frac{\partial \vec{B}}{\partial t} \quad (2.13)$$

$$\nabla \times \vec{H} = \vec{J}_{free} + \frac{\partial \vec{D}}{\partial t} \quad (2.14)$$

Here it is separated for the free and bound situation [12].

2.2 Landau-Lifshitz-Gilbert equation

The Landau-Lifshitz-Gilbert (LLG) equation is given by

$$\frac{d\vec{M}}{dt} = -\mu_0 \gamma \vec{M} \times \vec{H}_{eff} + \mu_0 \gamma \alpha \vec{M} \times \frac{d\vec{M}}{dt} \quad (2.15)$$

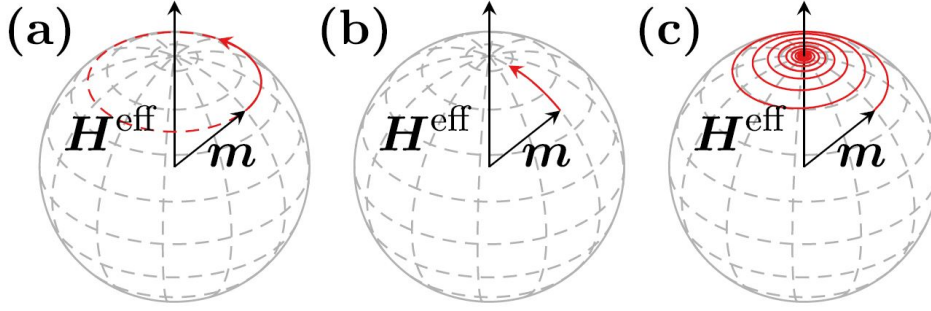


Figure 2.1: The phenomenon described by the LLG equation can be seen here. In (a) the precession of the magnetization m around the effective field H^{eff} is shown. In (b) the motion of m towards the effective field can be seen. In (c) both parts are added to give the spiral motion of the magnetization around H^{eff} (Graph taken from [1]).

The left side gives the time evolution of \vec{M} . The first term of the right hand side gives the precession of the magnetization because of the effective external field \vec{H}_{eff} . γ is the gyromagnetic ratio and given by $\gamma = \frac{ge}{2m_e}$ where g is the Landé splitting factor, e the elementary charge and m_e the mass of an electron. The second term is added because the effective field strives to align the magnetization with itself. α is the phenomenological Gilbert damping parameter.

The effective external field consists of multiple contributions which are an applied external field, the demagnetizing field and the anisotropy field. If there is no external field then \vec{H} is the stray field outside or the demagnetizing field inside the material given by equation 2.9. Magnetocrystalline anisotropy means the effect that some elements can be magnetized along specific crystallographic directions more easily. The anisotropy field is a concept which describes exactly that effect and points in the direction where the material is magnetized the easiest. The effective field also depends on the second spatial derivative of the magnetization divided by the volume [12].

The motion shown in figure 2.1 is described by the Landau-Lifshitz-Gilbert equation. In (a) the precession of the magnetization, here m , around the effective field H^{eff} is shown. In (b) the alignment of the magnetization with the effective field is depicted. Both effects combined give (c) where the spiral motion of the magnetization can be seen [1].

2.3 Characteristic impedance

A transmission line for the propagation of transverse electromagnetic waves consists of a minimum of two conductors. A lumped-element circuit can be used to describe one element of the line with length Δz . The circuit can be seen in figure 2.2. Here $i(z, t)$ and $v(z, t)$ are current and voltage as a function of position along the line z and time

2 Theoretical background

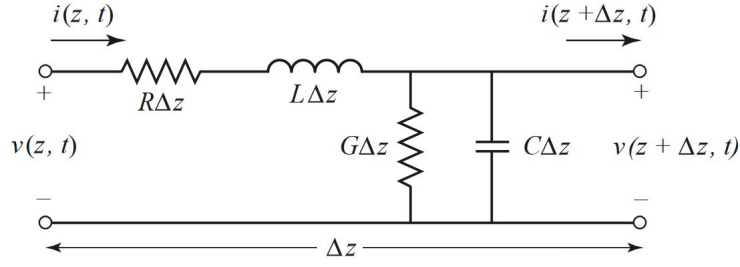


Figure 2.2: A lumped-element circuit as a model for a transmission line of length Δz (Graph taken from [16]).

t . R is the series resistance per unit length, L the series inductance per unit length, G the shunt conductance per unit length and C the shunt capacitance per unit length. The transmission line can then be described by the telegrapher equations.

$$\frac{\partial v(z, t)}{\partial z} = -Ri(z, t) - L\frac{\partial i(z, t)}{\partial t} \quad (2.16)$$

$$\frac{\partial i(z, t)}{\partial z} = -Gv(z, t) - C\frac{\partial v(z, t)}{\partial t} \quad (2.17)$$

These equations can be simplified with a sinusoidal steady-state condition and cosine-based phasors.

$$\frac{dV(z)}{dz} = -(R + j\omega L) I(z) \quad (2.18)$$

$$\frac{dI(z)}{dz} = -(G + j\omega C) V(z) \quad (2.19)$$

with the angular frequency ω and the complex number j . The two equations can be reformulated to

$$\frac{d^2V(z)}{dz^2} - \gamma^2V(z) = 0 \quad (2.20)$$

$$\frac{d^2I(z)}{dz^2} - \gamma^2I(z) = 0 \quad (2.21)$$

with the complex propagation constant γ given by

$$\gamma = \sqrt{(R + j\omega L)(G + j\omega C)} \quad (2.22)$$

The solution to the differential equations 2.20 and 2.21 are traveling waves in the form of

$$V(z) = V_0^+ e^{-\gamma z} + V_0^- e^{\gamma z} \quad (2.23)$$

$$I(z) = I_0^+ e^{-\gamma z} + I_0^- e^{\gamma z} \quad (2.24)$$

The exponential part of the first term of the right hand side describes the movement along positive z and the second one along negative z . Combining equation 2.18 and 2.23 yields

$$I(z) = \frac{\gamma}{R + j\omega L} (V_0^+ e^{-\gamma z} - V_0^- e^{\gamma z}) \quad (2.25)$$

and by putting this side to side with equation 2.24 the definition of the characteristic impedance Z_0 gives

$$Z_0 = \frac{R + j\omega L}{\gamma} = \sqrt{\frac{R + j\omega L}{G + j\omega C}} \quad (2.26)$$

The quantity Z_0 describes the relationship between the voltage and current along the transmission line [16].

2.4 Skin effect

In a circular conductor with total current $I = \cos(\omega t)$ where ω is the frequency and t the time the change in current gives rise to a changing magnetic field inside the conductor. The change in magnetic field causes eddy currents inside the conductor which circulate around the magnetic field lines. Increasing ω leads to an increase in magnetic field strength. The circulating eddy currents point in the direction of the total current around the periphery of the conductor and point in the opposite direction in the inner part. Thus the eddy currents weaken the current density in the middle of the conductor and strengthen it at the periphery. This is called the skin effect.

If ω is raised above a certain threshold then this leads to no current in the middle part and conduction is restricted to a band just below the surface. The thickness of the conducting band is then given by the skin depth δ_S by

$$\delta_S = \sqrt{\frac{2}{\omega\mu\sigma}} \quad (2.27)$$

μ is the magnetic permeability and σ the conductivity, both properties of the respective conductor [11].

2.5 Microstrip lines

The microstrip line is a type of planar transmission line for the transmission of hybrid transverse magnetic-transverse electric waves. Its advantages are among others the possible fabrication through photolithography and the miniaturization. In figure 2.3 a microstrip line can be seen. (a) shows the design. W is the thickness of the conductor placed on top of the dielectric substrate. Then the dielectric substrate in grey with thickness d and relative permittivity ϵ_r is the next layer and below that there is a ground layer. In (b) the microstrip line is viewed from the front with the conductor being the thick black line on top of the grey dielectric substrate. The electric field is visualized in black lines and the magnetic field in dashed lines.

The majority of the field lines are present in the dielectric substrate and a smaller part in the air beyond the material. If the thickness of the dielectric material is much smaller than the wavelength of the transmission line λ , meaning $d \ll \lambda$, then the solutions can be approximated by static or quasi-static ones. With the simplification the dielectric

2 Theoretical background

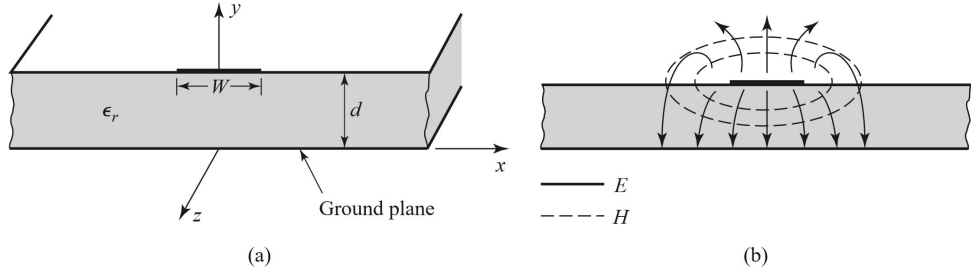


Figure 2.3: The schematic drawing of a microstrip line. In (a) the design is shown and important lengths and constants are indicated. The grey area is the dielectric substrate. In (b) this is viewed from the front. The electric field as black lines and the magnetic field as dashed lines are depicted here (Graph taken from [16]).

constant used to describe the system is the effective dielectric constant ϵ_e . For this it holds true that $1 < \epsilon_e < \epsilon_r$ and it is again caused by the field lines being partly in the dielectric substrate and partly in the air. The effective dielectric constant is calculated with

$$\epsilon_e = \frac{\epsilon_r + 1}{2} + \frac{\epsilon_r - 1}{2} \frac{1}{\sqrt{1 + 12d/W}} \quad (2.28)$$

This can be compared with a new homogeneous medium with dielectric constant ϵ_e which is in place instead of the air above and the dielectric substrate. Now the phase velocity v_p can be calculated with

$$v_p = \frac{c}{\sqrt{\epsilon_e}} \quad (2.29)$$

with c the speed of light [16].

3 Setup, material and methods

In this chapter the methodology of the experiment and the simulation is introduced. First the setup for the experiment is described and some key concepts like the scattering parameters (S-Parameters) are introduced. After that the software used for simulating is introduced and its workflow is discussed.

3.1 Experimental setup and methods

3.1.1 The experimental setup

In figure 3.1 the experimental setup can be seen. On the right there is the electromagnet. The two poles can be moved closer together or further apart by the bigger wheels on the left, one can be seen in the middle of the figure. In the picture one set of microstrip antennas is already between the electromagnet. It is attached to a holder and the holder is then suspended between the two poles by moving them together. On one side the set of microstrip antennas is screwed to the holder. Beforehand it is screwed to a set of end-launch connectors which lay on the ends of the single microstrip antennas. On the other side, to keep the antennas as flat as possible, it is taped to the holder. The end-launch connectors are then connected with the coaxial cables and a screw is tightened lightly. The other end of the coaxial cables is connected to the vector network analyzer (VNA) which sends the signal through the cable to the end-launch connectors and then to the microstrip antennas. When measuring outside the magnet the holder can just be placed on the table, but it has to be made sure that the cables do not bend too much. For measurements in the electromagnet it is important to place the set of antennas very close to the center of the magnetic field in the electromagnet. After that a Hall probe is placed closely above the antennas to measure the magnetic field strength. Additionally for some measurements a Yittrium Iron garnet (YIG) waveguide is put onto the microstrip antennas laying across the distance between and perpendicular to them. In the material a spin wave is induced. YIG has low magnetic damping and thus spin waves can propagate through it over a distance of some cm [18]. The waveguide used here has a thickness of $7.78\ \mu\text{m}$ and the core is made of Gadolinium Gallium garnet (GGG) where the YIG is grown fully around it using liquid phase epitaxy.

3.1.2 Vector network analyzer and scattering parameters

The vector network analyzer (VNA) employed for the experiment is the Anritsu MS4642B which can be seen on the left of figure 3.1. It is controlled by the *VectorStar* program installed on it. The VNA can send a signal to one microstrip antenna and receive the

3 Setup, material and methods

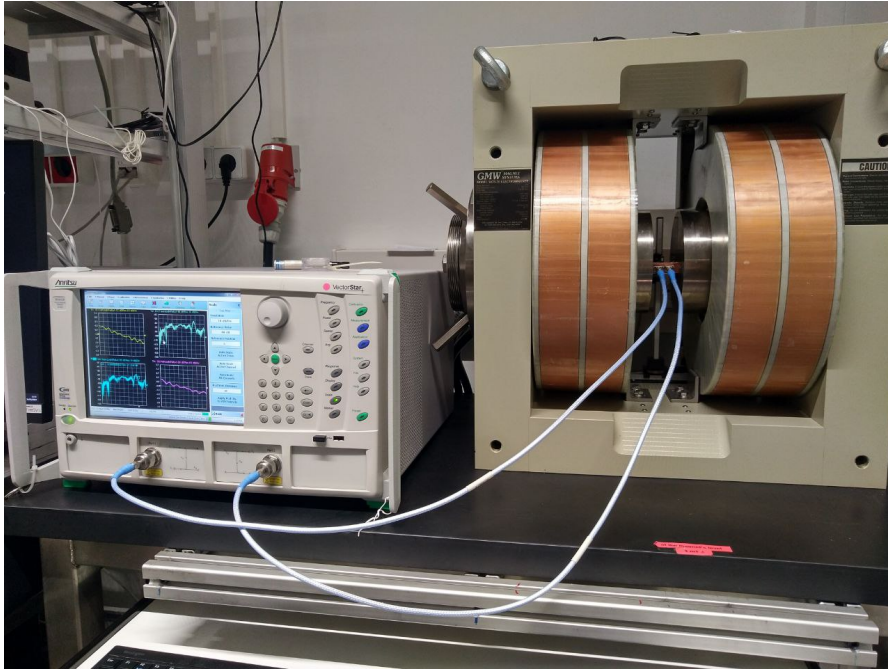


Figure 3.1: The experimental setup is shown here. On the left is the VNA already displaying a measurement and on the right is the electromagnet with a set of microstrip antennas between the poles. The two are connected by coaxial cables.

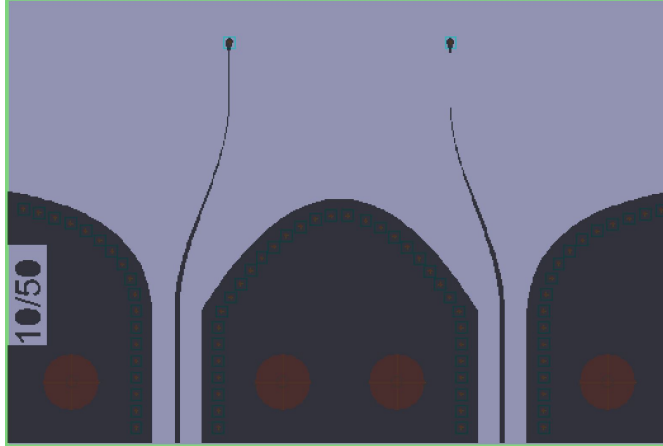
transmitted and reflected signal. The inputted signal will be referred to as Port 1 and the received as Port 2, thus this is a two port setup. Additionally to sending and receiving the signal another advantage of the VNA is that it can sweep a specific frequency range, going from 10 MHz to 20 GHz.

What the VNA returns are the scattering parameters (S-Parameters) which are determined by recording the received signal and the signal that was reflected from the inputted signal. They are transformed into a digital signal and then the S-Parameters are calculated and shown on the display of the VNA. The S-Parameters are a function of frequency, so this has to be done for every frequency that is inputted as a signal and the S-Parameters are plotted against the frequency. For a two port setup there are four S-Parameters where S_{ii} describe the reflection of the incoming signal back to the source in Port 1 ($i = 1$) or Port 2 ($i = 2$). S_{21} and S_{12} then describe the transmission of a signal between the two ports. The S-Parameters are given here in dB with the conversion of $S_{ij} = 20 \log_{10} |S_{ij}|$.

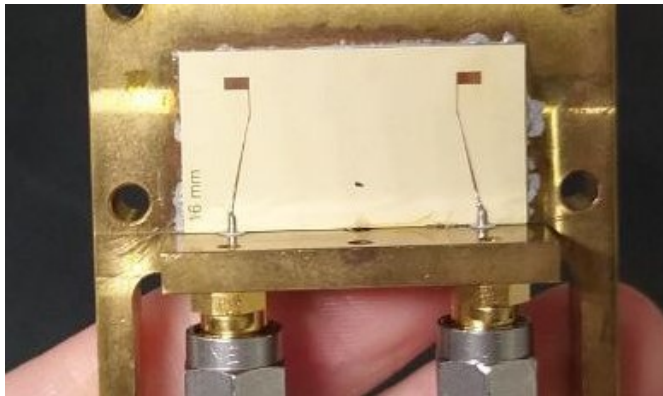
The VNA and the connected coaxial cables have to be calibrated first. This is done to account for phase delay in the cables and to maximize the accuracy of the impedance measurements. The settings for calibration are chosen in the VNA and both cables alone

3.1 Experimental setup and methods

are calibrated and both together [19]. The chosen power here and for all measurements is $0 \text{ dBm} = 1 \text{ mW}$. The whole frequency range is used and the number of measurement points is 25 000.



(a) 10 mm distance set of microstrip antennas with real direct ground.



(b) 16 mm distance set of microstrip antennas with capacitor-like ground.

Figure 3.2: Two of the sets of microstrip antennas. On top a technical design of the set of microstrip antennas is shown and on the bottom an image of one with holder, end-launch connectors and screws of the coaxial cables can be seen.

3.1.3 Measurements

The measurements are done with three different sets of antennas. Two sets of microstrip antennas with real direct ground and a distance between the antennas of 4 mm and 10 mm and one set with 16 mm distance and a capacitor-like ground. Two of them can be seen in figure 3.2. On top the technical design of the set of antennas with 10 mm distance between them and real direct ground is shown. The numbers on the left indicate the

3 Setup, material and methods

distance and the characteristic impedance of the microstrip lines. Below a picture of the set with 16 mm distance between the antennas and capacitor-like ground is visible. What can also be seen in the picture is the holder in the background, the connection on the microstrip antennas by the end-launch connectors and the screws of the coaxial cables. The first measurements are done with the set of microstrip antennas with the 4 mm distance between. After calibration and connecting the VNA and the set the holder is placed on the table and the S-Parameters for the defined frequency range are measured and saved.

Then the set and the holder are brought into the electromagnet. Three options concerning the geometry are possible. Along the magnetic waveguide, here YIG, the spin wave propagates throughout the longer side of it from one antenna to the other. The propagation direction of the spin wave points along the longer side of the waveguide. If the external magnetic field is perpendicular to the propagation direction this gives rise to forward volume magnetostatic spin waves (FVMSW). The magnetization is out of plane. For in plane two configurations can be defined. For an external field which points in the same direction as the propagation direction that is referred to as backward volume magnetostatic spin waves (BVMSW) and if the two directions are perpendicular then it is referred to as magnetostatic surface spin waves (MSSW) [18]. Even though not all measurements include YIG as magnetic waveguide some measurements in the electromagnet are conducted with different orientations of the set of antennas and the holder. Here a similar naming convention is used. If the measurement would result in BVMSW then this is referred to as backward volume geometry (as there are no MSWs present). Likewise FVMSW geometry is called forward volume geometry and the MSSW just surface geometry. If the YIG is present the measurement method is called propagating spin wave spectroscopy. For forward volume and surface geometry U-shaped end-launch connectors are used so that the coaxial cables do not get in the way.

The first set of microstrip antennas is brought into the electromagnet in the backward volume geometry and it is measured without an external magnetic field. Then an external field is applied at 1.25 T and the parameters are measured. The results are saved and the same is done with a field of 350 mT. After that for the second field the YIG waveguide is placed on top of the antennas and again it is measured and saved. All this is then done in the forward volume geometry, besides the measurement with YIG which is not possible given the geometry of the setup, and in the surface geometry, but here the external magnetic fields used are 1.016 T and 350 mT. The measurements outside of the magnet and inside the magnet with and without magnetic field in backward volume geometry and with and without YIG in BVMSW configuration are then done for the 10 mm distance set of microstrip antennas with real direct ground and 16 mm distance set of microstrip antennas with capacitor-like ground.

3.2 COMSOL Multiphysics

The software used for the simulations is COMSOL Multiphysics. This program provides a full workflow, from modelling the device in the program to adding the physics and

Table 3.1: The dimensions of the model in COMSOL for the 10 mm distance set of microstrip antenna. The first column gives a name and the third a description of the length stated. The second column gives the value in mm or in mil if stated.

Name	Value (mm)	Description
width	30	Width of the dielectric base
depth	20	Depth of the dielectric base
thickness	10 mil	Thickness of the dielectric base
length bottom	6.387	Length of the bottom straight part of the antenna
width bottom	0.229	Width of the bottom straight part of the antenna
indentation bottom	7.55	Indentation for the bottom straight part of the antenna
diameter	0.305	Diameter of the real direct ground
offset	1.71	Offset of the real direct ground
indentation circle	9.83	Indentation for the real direct ground
length top	2.802	Length of the top straight part of the antenna
width top	0.04	Width of the top straight part of the antenna
indentation top	9.96	Indentation for the top straight part of the antenna

Table 3.2: The material properties for the two materials used.

	Air	GGG
Relative permeability	1	1
Relative permittivity	1	11
Electrical conductivity (S m^{-1})	0	0

evaluating the results. Here only the 4 mm and 10 mm distance sets of microstrip antennas are simulated and compared with the experimental results. Also only the measurement outside the magnet is recreated in COMSOL.

The first step is modelling and building the device. The program gerbv¹ is used to view the technical design of the microstrip antennas. In this program the antennas can be measured out and their dimensions are inputted in COMSOL and rebuilt. The values for the 10 mm distance set of microstrip antennas can be seen in table 3.1. In the first column a name is given and in the last one a description. In the second column the numerical values are listed in mm if not stated otherwise. Bottom and top refer to the straight parts of the microstrip antenna below or above the curved part and circle to the real direct ground at the end of the antennas (see figure 3.2). Indentation refers to the distance from the left side of the model and offset from the top end. The model can be seen in figure 3.3. Here the antennas can be seen on top of a rectangular box. This is the dielectric material. Also a box around the antennas and the dielectric material is visible which is used to simulate the situation in the lab with an environment around it.

¹<http://gerbv.geda-project.org/>

3 Setup, material and methods

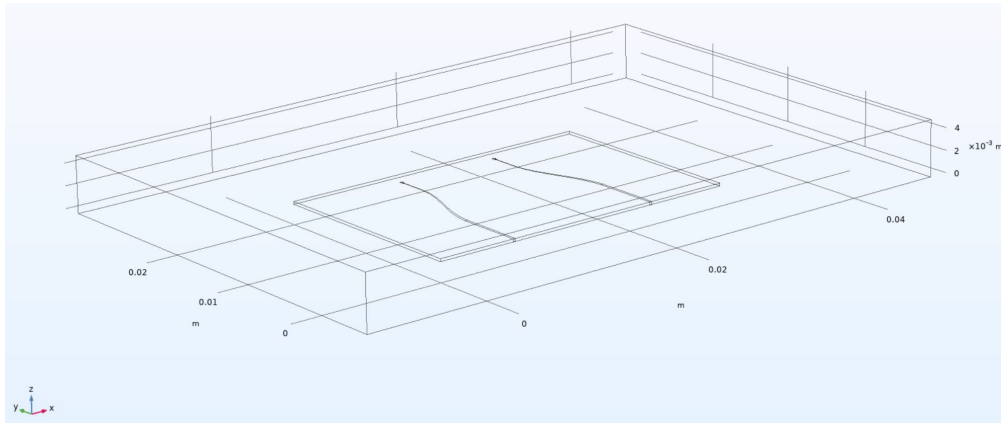


Figure 3.3: A picture of the three dimensional model from COMSOL for the 10 mm distance set of microstrip antennas.

In COMSOL materials can be assigned to the different parts of the model. With this important material properties and constants are selected for the parts and are used in simulating. The box around the dielectric material and the antennas is assigned the built-in air. For the dielectric base GGG is used here. The material properties needed and their values are listed in table 3.2.

For the physics the *Electromagnetic wave, Frequency domain* is employed which solves for the time-harmonic electromagnetic field distribution. For simulating the connection of the microstrip antennas with the end-launch connectors two lumped ports are used. These model a transmission line or current source [9]. The first lumped port represents where the signal is induced and a power of 1 mW is set as input with a characteristic impedance of $50\ \Omega$. The second port receives the signal and here just the characteristic impedance is defined. One important simplification that is made for the simulation model is the perfect electric conductor (PEC). This boundary condition simulates a surface which has no losses [10]. As was shown a microstrip antenna would consist of a ground plane, a layer of dielectric material and the antennas. Here the ground plane and the antennas are modelled as PEC. Because of this the geometry of the antennas is just modelled in two dimensions on top of the dielectric layer and the bottom surface of the dielectric base where the ground plane would lie is also assigned a PEC condition as a whole.

For numerically solving the equations the model has to be discretized. A mesh is built which consists of tetrahedals. Here the physics-controlled mesh of COMSOL is chosen. In this case COMSOL itself evaluates the physics and builds a mesh that is optimized for the problem at hand. The information comes from added knowledge into the application [8]. The last step, the study step, defines how the problem will be solved. Here two approaches are made. First the *Frequency Domain* which solves a linearized model when excited harmonically for specific frequencies is simulated. It then solves for the induced signal its transmission and reflection and returns this in the form of S-Parameters for each frequency step [6]. The frequency range is from 100 MHz to 20 GHz in steps of 100 MHz.

3.2 COMSOL Multiphysics

The second study consists of the steps *Eigenfrequency* and *Frequency Domain, Modal*. The first step searches for the resonant frequencies and the normalized electromagnetic field at these frequencies [5]. The second step again solves a model just like the first study, but only for the resonant frequencies [7]. The frequency range for searching for eigenfrequencies and for the second step is the same as for the first study.

4 Results

This chapter presents the results of the experimental and numerical studies and these will be placed next to each other for comparison. First the results of the 4 mm distance set of microstrip antennas will be shown and then the comparison of them with the other sets of antennas with different distance and ground. Next the measurement results are compared with the simulation and the features of the simulation results will be analyzed in more detail.

4.1 Experimental results

4.1.1 4 mm distance set of microstrip antennas in different geometries

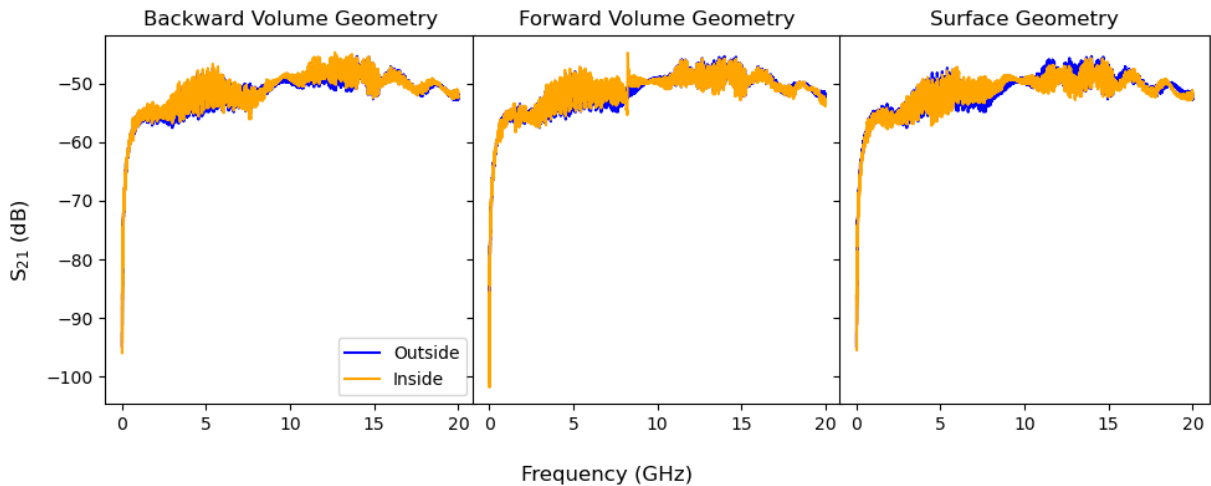


Figure 4.1: Measurements of the 4 mm distance set of microstrip antennas outside the magnet in blue and inside the magnet without an external field in orange. The title of the plot indicates the measured geometry. The frequency in GHz is given on the x-axis and S_{21} in dB on the y-axis.

The measurement results for the 4 mm distance set of microstrip antennas outside the magnet and in comparison with inside the magnet without an external magnetic field in all three geometries is shown in figure 4.1. On the y-axis is the S_{21} parameter in dB and on the x-axis the frequency in GHz. The blue graph always denotes the measurement

4 Results

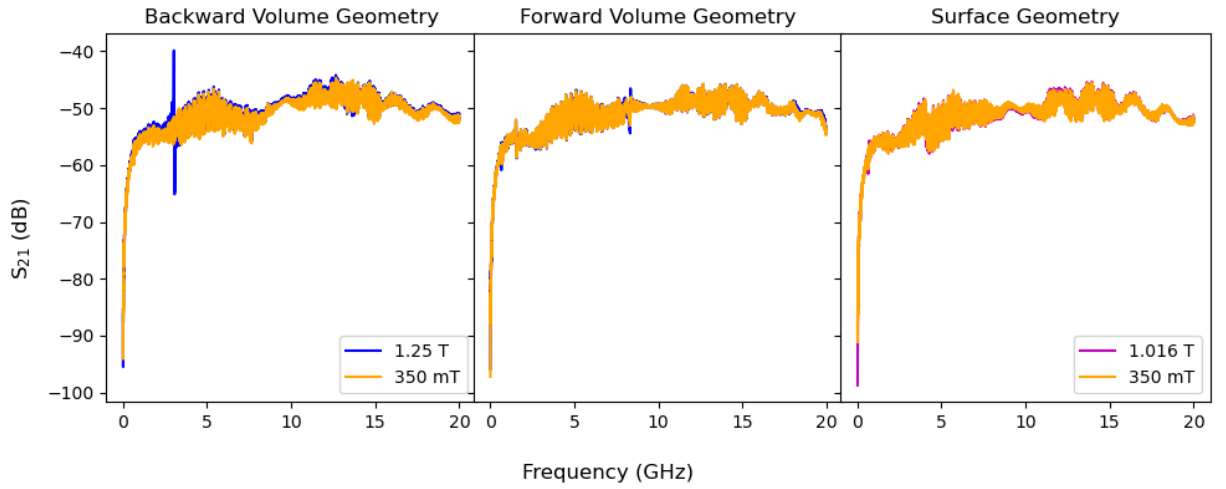


Figure 4.2: Measurements of the 4 mm distance set of microstrip antennas inside the magnet with two different field strengths in blue and orange and for the surface geometry in magenta as the field strength is different here (see legend of the plots for the values). The title of the plot indicates the measured geometry. The frequency in GHz is given on the x-axis and S_{21} in dB on the y-axis. Here no YIG waveguide is present.

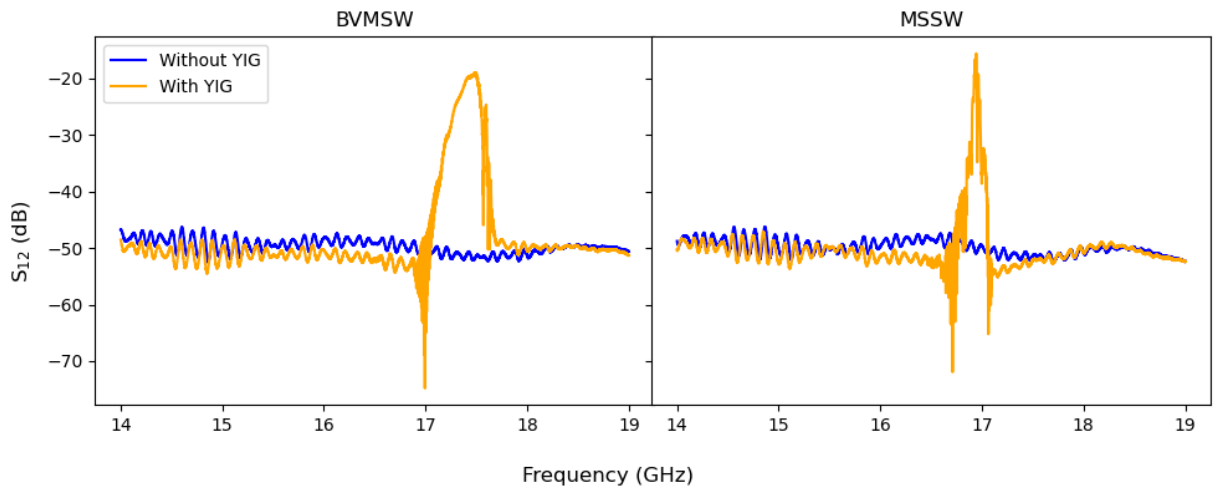


Figure 4.3: Measurements of the 4 mm distance set of microstrip antennas inside an external field of 350 mT with the YIG waveguide on top of it in orange and without in blue. Here the x-axis is the same as before, but only a part of the spectrum is shown, and the y-axis in dB shows the S_{12} parameter.

outside and the orange inside the magnet, the geometry is given in the title of each plot. What can be seen in the respective plots is the transmission of the electromagnetic wave in the frequency range of 10 MHz to 20 GHz. For very small frequencies up until 1 GHz there is a steep increase in the value of S_{21} and continues in a stable value between -60 dB and -50 dB which states that there is some leakage. This fits for all three graphs regardless of measured geometry. For forward volume geometry in the middle plot a peak for inside the magnet can be seen around 8 GHz.

In figure 4.2 the measurement results for the 4 mm distance set of microstrip antennas in all three geometries with two different external magnetic field strengths can be seen. The blue graph is for 1.25 T and the orange one for 350 mT. The measured geometry is again given in the title of the plot. For the surface geometry one graph is magenta because here it was measured with a different larger field strength of 1.016 T compared to the other geometries. The axis are the same as in the figure before. This measurement does not include a YIG waveguide, so no MSW signal is present here. The frequency range is identical to the previous plot and the courses of the graphs are the same with a steep increase up to 1 GHz and a stable electromagnetic leakage with values between -50 dB and -60 dB for the S-Parameter. Again for forward volume geometry the small peak can be seen in the middle, but only for the stronger magnetic field and for this one in the backward volume geometry a strong peak is visible around 3 GHz.

The measurements of the 4 mm distance set of microstrip antennas with and without the YIG waveguide placed on top of the antennas and in an external field of 350 mT is shown in figure 4.3. The blue graph is without the waveguide and the orange one with. Here the frequency in GHz is again shown on the x-axis, but it is just a cut of the whole spectrum between 14 GHz and 19 GHz to display the features. The title of the plots gives the MSW that is excited here, left BVMSW and on the right MSSW. On the y-axis here S_{12} is shown which is used because for the case of MSSW the S_{12} and S_{21} parameter are not symmetric as they are not volume waves, but for BVMSW they are. The switch in parameter comes from switching which cable is connected to which end-launch connector. For decreasing frequency the graph of the BVMSW and with that the transmission of the electromagnetic wave also decreases. The microstrip antennas have decreasing excitation and detection efficiency at lower frequencies which are the causes of this. The peak of the graph marks the spin wave where the wave vector converges to 0 and the transmission value of -50 dB left and right of the peak is due to the electromagnetic leakage. For the MSSW the effect of decreasing frequency and decreasing transmission holds here as well [18].

4.1.2 Comparison of the results for the structures under investigation

In figure 4.4 the measurements of all three sets of microstrip antennas are shown, the 4 mm and 10 mm distance with real direct ground and the 16 mm distance with capacitor-like ground. Here the measurements of outside the electromagnet in blue and inside without an external field in backward volume geometry in orange are presented. The x-axis gives the frequency in GHz and the y-axis the S_{21} parameter in dB. The title of the plot states which set is shown here. The description of the measurement for the 4 mm distance set is

4 Results

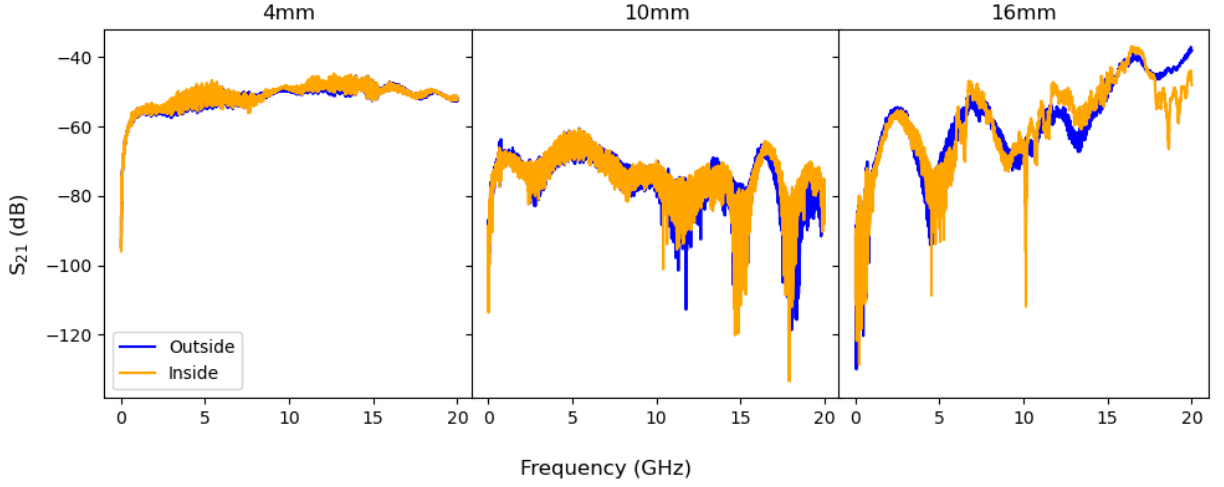


Figure 4.4: Measurements of the three sets of microstrip antennas outside in blue and inside the electromagnet without an external field in orange. The different distances between the single antennas is given in the title of the plots. The frequency in GHz is given on the x-axis and S_{21} on the y-axis in dB.

given in the section before. The 10 mm distance set has a steep increase up to 1 GHz and stays between -60 dB to -80 dB up to 10 GHz where some features are already visible. These become more pronounced after that and cause a wider range of S_{21} to be covered up until 20 GHz. The 16 mm set has the same steep increase, but stronger features are visible up to 10 GHz. From that on an increase from -70 dB to -40 dB can be seen. The measurements of all sets of microstrip antennas inside the electromagnet with two different external fields applied can be seen in figure 4.5. The blue graph is for a field strength of 1.25 T and in orange for 350 mT. For the 16 mm distance set of microstrip antennas a different field strength is used with a value of 1.2493 T which is displayed in magenta. The axis and the title of the plots are the same as before. Again no YIG waveguide is used. The description for the 4 mm distance set is given in the section before and the description of the other two sets holds true from the last paragraph for here as well. Some peak-like features can be seen for the set of antennas with the largest distance and again the peak around 3 GHz is visible for the smallest distance set.

The measurement results for the three sets of microstrip antennas with and without the YIG waveguide are shown in figure 4.6. The external field has a strength of 350 mT. The blue graph shows the measurement without the waveguide and the orange one with. The title and axis are the same as before, but again the x-axis only shows a part of the spectra. For the 4 mm distance set of microstrip antenna the x-axis goes from 15 GHz to 19 GHz, for the other two from 10 GHz to 14 GHz. An explanation of the slope for the BVMSW for the 4 mm distance set is given in the section before, but it holds true for the larger distances between the antennas. However for the 10 mm distance set the increase is sharp

4.2 Comparison of the simulation and the experimental results

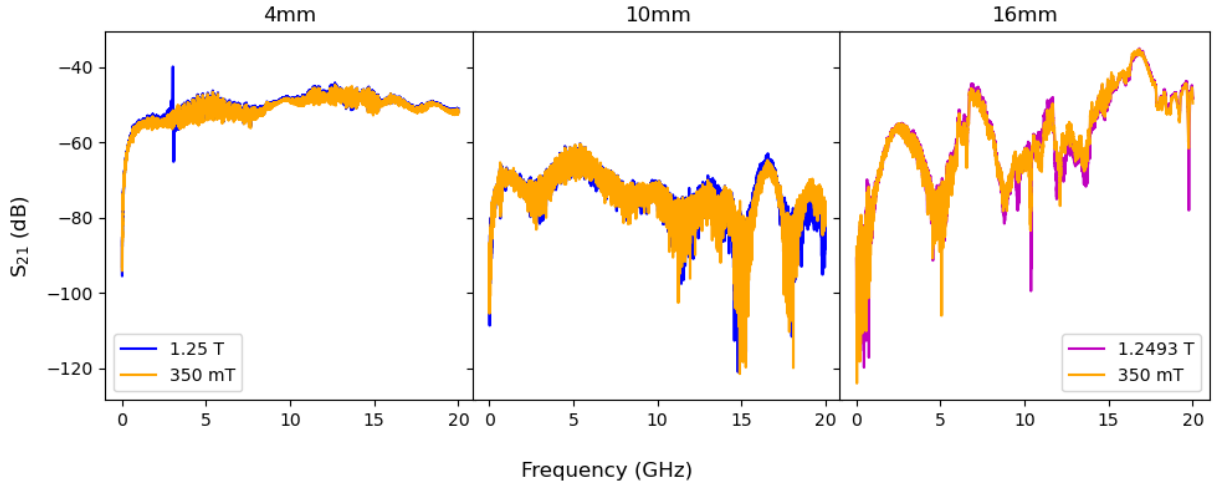


Figure 4.5: Measurements of the three sets of microstrip antennas inside the magnet with two different field strengths in blue and orange and for the largest distance between the antennas on the right in magenta as the field strength is different here (see legend of the plots for the values). The y-axis shows the S_{21} parameter in dB, the x-axis the frequency in GHz and the titles indicate the distance of the used set of antennas. Here no YIG waveguide is present.

and for the largest distance set it is more noisy and sharp.

4.2 Comparison of the simulation and the experimental results

The two different studies which were described will be referred to as Study 1 for the *Frequency Domain* and Study 2 for the study including the determination of the eigenvalues. COMSOL returns both the S_{11} and S_{21} parameter, so these two will be compared to their respective measurement results.

In figure 4.7 the comparison of the results of the experiment and the simulation for the 4 mm distance set of microstrip antennas can be seen. In the left plot the S_{11} parameters are compared against each other and on the right the S_{21} parameter, they are given on the respective y-axis in dB. In both plots the x-axis is the frequency in GHz from 10 MHz for the experiment and 100 MHz for the simulation to 20 GHz for both. The simulated results are given as scatter plot indicating the frequencies for which the model was solved. The S_{11} parameter stays constant for the simulation and decreases for the experimental results. For the S_{21} parameter the steep increase at low frequencies can be reproduced in the numerical results and stays constant a bit above the experimental ones around -40 dB to -50 dB.

4 Results

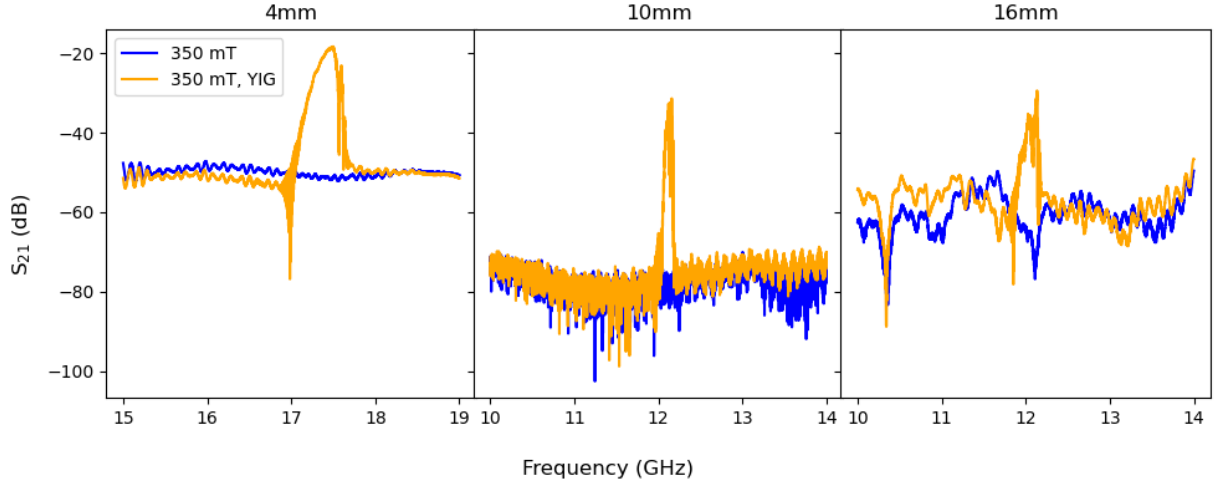


Figure 4.6: Measurements of the three sets of microstrip antennas inside an external field of 350 mT with the YIG waveguide on top of it in orange and without in blue. The x- and y-axis are the same as before and the title states the distance of the measured set of antennas. However the frequency range is different for the left plot from the rest, the middle and right one have the same range.

The exact same plot for the 10 mm distance set of microstrip antennas can be seen in figure 4.8. The description for the S_{11} parameter is the same and for the S_{21} parameter the simulation results lie between -60 dB and -70 dB close to the experimental ones.

It can be seen that the simulation results have multiple peaks in them which are not reproduced in the experimental data. This can be caused by resonances in the model which are due to standing waves and their respective overtones $n \cdot \lambda$ of the wavelength λ , with n being an integer or the inverse of an integer. The wavelength of the peak can be determined with the simulation data and the equation for velocity v , wavelength and frequency ν of a wave, $v = \lambda\nu$. The peaks are found using the *python* function *scipy.signal.find_peaks* and the step size of the simulation of 100 MHz is taken as uncertainty for the found values. The velocity used here is the phase velocity v_p and it is calculated with equation 2.29 with the value for the speed of light of $c = 3 \cdot 10^8 \text{ ms}^{-1}$. As the width of the microstrip antenna changes ϵ_r is used for the calculation as an upper bound. With this the length scales are calculated and are then used as lower bounds. For the 4 mm distance set of antennas the settings used for finding the peaks are *height* = -45 , *distance* = 25, *threshold* = 5. The first value is negative as the function takes the inputted y-values for the S_{21} parameter and uses it as a lower bound for the peaks. With the settings both studies yield the same results which are listed in table 4.1. In the first column the found peak frequencies in GHz are given with the uncertainty and in

4.2 Comparison of the simulation and the experimental results

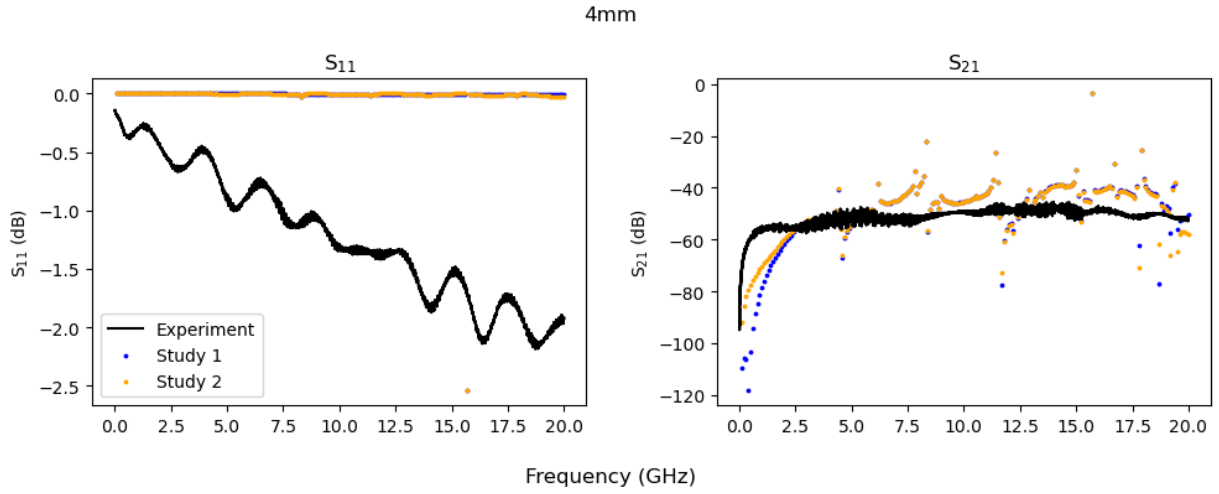


Figure 4.7: The results for the experiment and the simulation for the 4 mm distance set of microstrip antennas. In black the experimental result, in blue the results for Study 1 and in orange for Study 2 can be seen. The x-axis displays the frequency in GHz and on the left the y-axis shows the S_{11} and on the right the S_{21} parameter, both in dB.

Table 4.1: The peaks for the 4 mm distance set of microstrip antennas for both Study 1 and Study 2.

Frequency (GHz)	λ (mm)
4.4 ± 0.1	20.56 ± 0.47
8.3 ± 0.1	10.90 ± 0.14
11.4 ± 0.1	7.935 ± 0.070
15.7 ± 0.1	5.761 ± 0.037

Table 4.2: The peaks for the 10 mm distance set of microstrip antennas for both Study 1 and Study 2.

Frequency (GHz)	λ (mm)
6.2 ± 0.1	14.59 ± 0.24
8.3 ± 0.1	10.90 ± 0.14
11.4 ± 0.1	7.935 ± 0.070
15.7 ± 0.1	5.761 ± 0.037

the second column the length scales in mm. The settings of the function for the 10 mm distance set of microstrip antennas are $height = -40$, $distance = 21$, $threshold = 5$ and again both studies have the same result which is shown in table 4.2 with the same columns.

4 Results

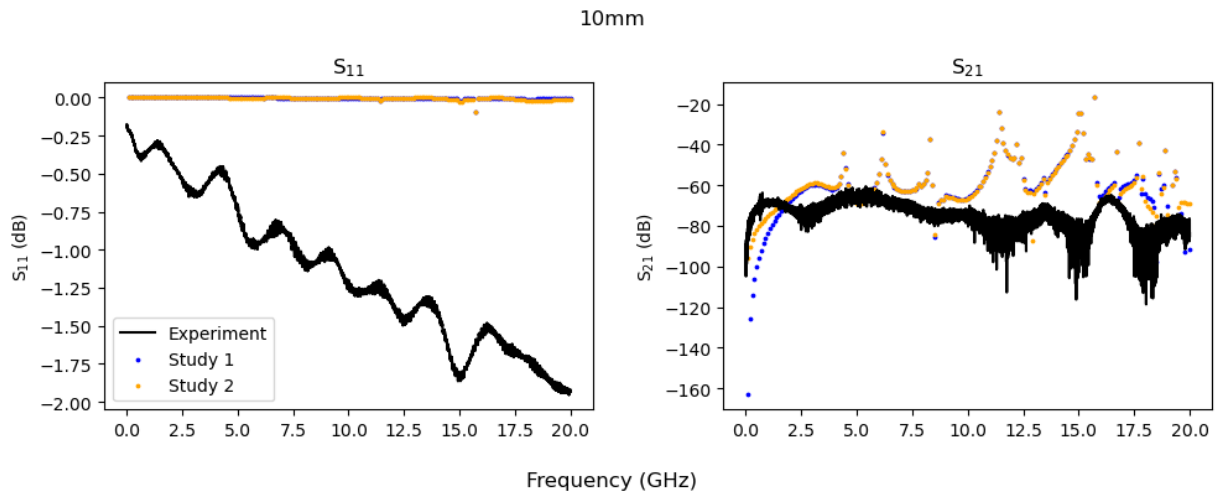


Figure 4.8: The results for the experiment and the simulation for the 10 mm distance set of microstrip antennas. In black the experimental result, in blue the results for Study 1 and in orange for Study 2 can be seen. The x-axis displays the frequency in GHz and on the left the y-axis shows the S_{11} and on the right the S_{21} parameter, both in dB.

For both sets of microstrip antennas and both studies the simulation results are again plotted in figure 4.9 in blue. Additionally shown here as black dots are the found peaks. In the title the set of microstrip antennas and study presented are indicated. The y-axis shows the S_{21} parameter in dB and on the x-axis the frequency in GHz is shown.

4.2 Comparison of the simulation and the experimental results

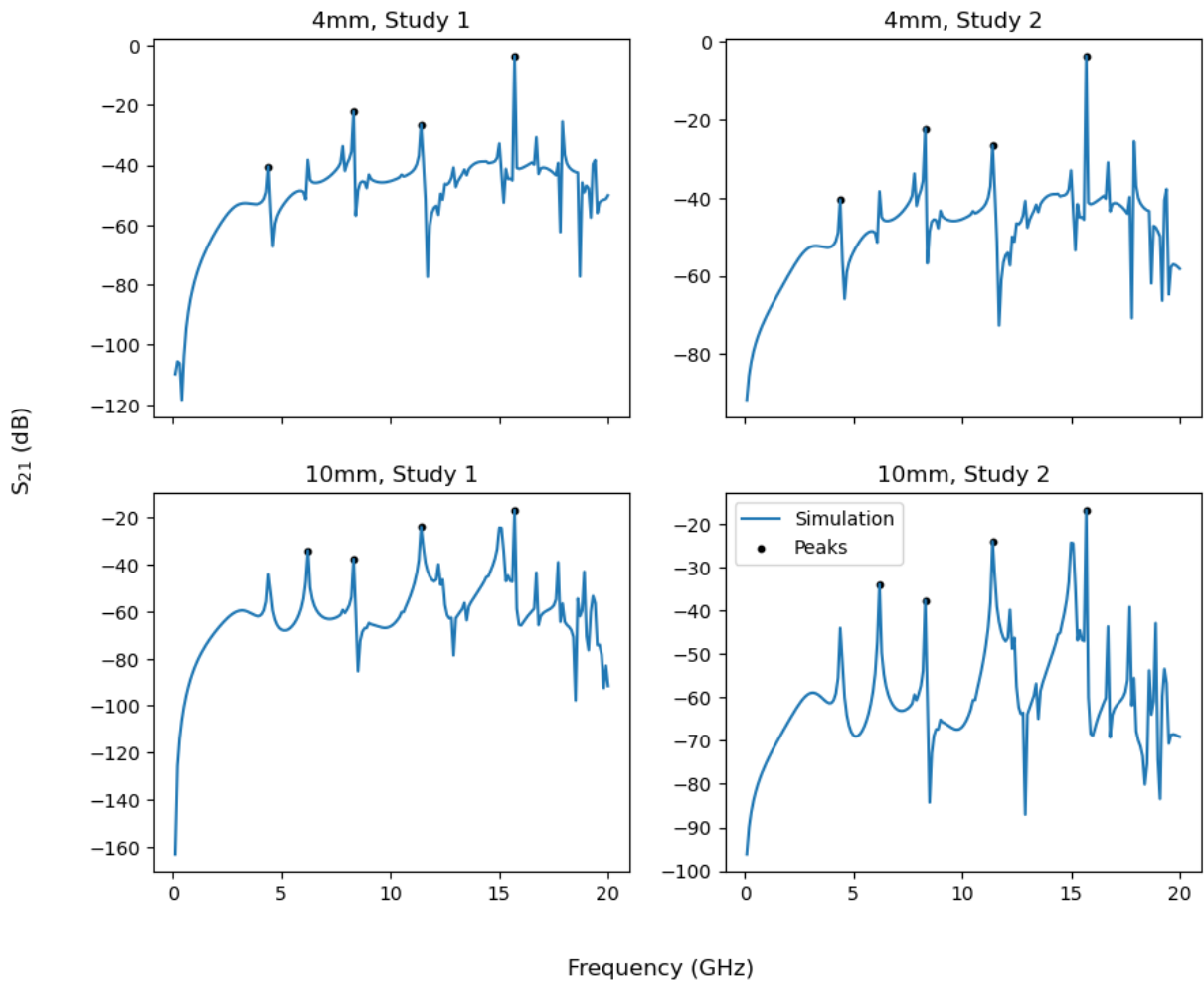


Figure 4.9: The results for the S_{21} parameter for both sets of microstrip antennas and both studies. The title of the single plots states which set of microstrip antennas and study is shown. The blue graph is the simulation result and the black dots indicate the found peaks. The legend in the lower right plot is valid for all of them. The x-axis displays the frequency in GHz and the y-axis S_{21} in dB.

5 Discussion

In this chapter the just presented results will be discussed and analyzed further. First the experimental results of the 4 mm distance set of microstrip antennas will be discussed and deviations will be explained. Afterwards the discussion continues with the measurements of the three sets of microstrip antennas with different distances between the antennas and ground types. Lastly the comparison of experimental and numerical results is going to be debated and the cause of the peaks and resonances will be determined.

5.1 4 mm distance set of microstrip antennas in different geometries

In figure 4.1 it can be seen that the presence of the electromagnet itself does not change the transmitted signal. It was unsure if the poles could influence the wave transmission and cause a change in the S_{21} parameter. However as all graphs lay pretty much on top of each other it is safe to assume that this is not the case for any geometry. For all three of them the blue and orange graphs pretty much lay on top of each other with the strongest deviation for the surface geometry. Additionally all the graphs have the same shape, even among the different geometries. Starting with a steep increase followed by a broader region and going into a thinner width, ending in again a broader region with more wave like features and ending in a smaller stripe. This shape can be seen for all six graphs. What is not expected here is the small peak for forward volume geometry around 8 GHz. This causes a larger deviation from the results form outside the electromagnet. The reason can not fully be determined, the peak could be due to the formation of a standing electromagnetic wave between the poles of the electromagnet. What can also never be ruled out are measurement errors. Additionally the VNA would have an averaging function where the returned measurement results are averaged over multiple measurements, but it was not used here. For an exact analysis of the peak further measurements would be needed. What can be performed afterwards is smoothing of the experimental data. Using a Savitzky-Golay filter¹ in the form of the *python* function `scipy.signal.savgol_filter` the experimental data is smoothed in an attempt to remove this peak. The smoothed graph can be seen in figure 5.1 with the geometry and the setting of the filter in the title of the plot. The axis are the same as for figure 4.1, but just a part of the y-axis range is visible from -60 dB to -45 dB. Here a faint signal of the peak can still be seen, but the overall course of the graph now matches the graph of the measurement outside the electromagnet.

¹For an exact description of this filter see [17]

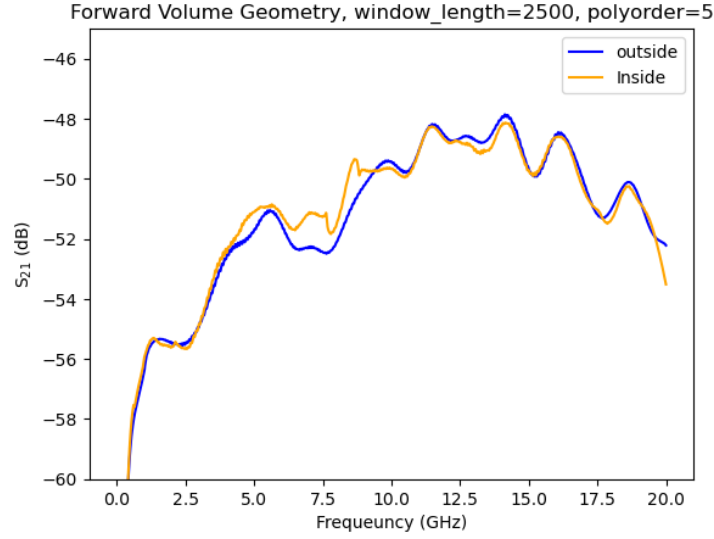


Figure 5.1: The smoothed experimental results of the measurements of the 4 mm distance set of microstrip antennas in the forward volume geometry. For axis and color descriptions see figure 4.1. The settings of the filter are given in the title of the plot. Here just a part of the y-axis range is shown.

For the comparison of the effects of different field strengths a similar picture applies. All three graphs of the different geometries overlap very well, nevertheless which field strength is applied. The surface geometry overlaps almost perfectly, but a different larger field strength is applied here. The results for the forward volume geometry overlap very well, but again the small peak is present for the larger external field strength. Also a very strong peak for the backward volume geometry measurement is present. The cause of both can again be debated, the same assumptions as before apply. For the larger peak an attempt of smoothing it out is again made. The result can be seen in figure 5.2. The axis description, title and the y-axis range is the same as for figure 5.1. The blue graph is for 1.25 T and the orange one for 350 mT. Again the peak disappeared and the two graphs overlap or follow the same slope with a small difference between them. Thus the different field strengths do not cause a difference in the transmitted signal when no YIG waveguide is present.

The effect of the YIG waveguide can be seen in figure 4.3 which causes a visible peak at a specific frequency while the measurement without it does not display any specific features. The peak for the BVMSW configuration is broader and less noisy while the peak for MSSW is narrow, but steeper in increase. Both have a steep decrease and a stronger signal pointing downwards at the left beginning of the peak. The orange graph for BVMSW left to the peak is lower than the blue graph which should not be the case. Besides for the

5.2 Comparison of the results for the structures under investigation

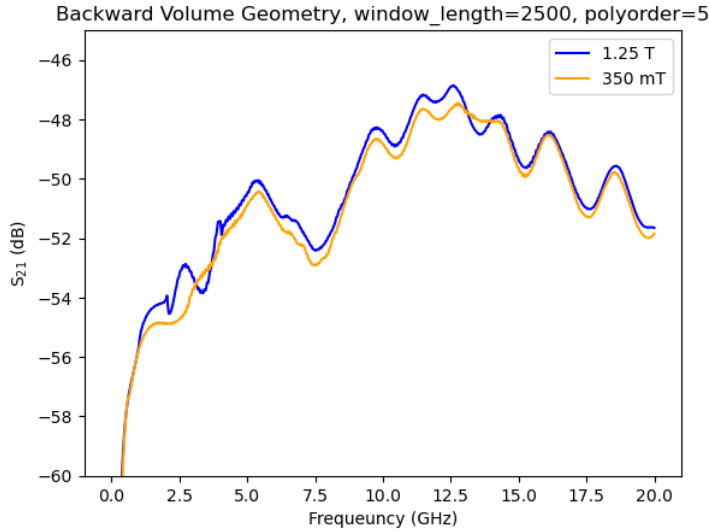


Figure 5.2: The smoothed experimental results of the measurements of the 4 mm distance set of microstrip antennas in backward volume geometry. For axis and color descriptions see figure 4.2. The settings of the filter are given in the title of the plot. Here just a part of the y-axis range is shown.

peak the two graphs should again overlap. The cause of this is not fully clear. Maybe a loss of power in the YIG waveguide before the peak can cause the difference. Another possible explanation is that the GGG serves as waveguide for an electromagnetic wave due to its large relative permittivity. On the right side of the peak at first the orange graph is shortly higher which can still be caused by the peak and then overlaps with the blue graph again as expected. For the MSSW configuration at first both graphs overlap as it should be. However shortly before the peak the orange graph is again below the blue one which happens again right after the peak and then both overlap. The cause can again be attributed to a possible loss in power due to the YIG, but without a signal peak. Also external influences could cause this or an unstable magnetic field possibly.

5.2 Comparison of the results for the structures under investigation

The comparison of the transmitted signal for the three different sets of microstrip antennas is shown in figure 4.4. The measurement for the 4 mm distance set of antennas is explained in the section before. What can be seen for growing distance between the antennas is that the results get more noisy and more slopes are present. Because of that the overlap is not as good anymore as it was for the case before. However for the 10 mm distance set of microstrip antennas the overlap is still sufficient between the orange and the blue

5 Discussion

graphs. For larger frequencies more features are present, but this is the case for in- and outside the electromagnet. The lower values for the S_{21} parameter can be explained by more loss during the propagation over a larger distance. For the 16 mm distance set of antennas the description is the same. More features are present especially in the middle of the plot. Also the overlap is not that great here and a peak pointing downwards can be seen. As already shown the peak can be smoothed out. At the right end of the plot both graphs lay on top of each other again, but then the orange graph deviates to smaller values in comparison to the blue graph. What can also be seen is that the graphs for out- and inside the magnet increase in value with increasing frequency. This cannot be attributed to the increase in distance between the antennas. It could be caused by the different capacitor-like ground with respect to the other sets with real direct ground.

For the effect of two different external field strengths in figure 4.5 again for 4 mm and 10 mm distance sets of antennas no difference to the case without a field or a magnet can be seen and the graphs overlap very well for these two, again a bit worse for the larger distance between the antennas. For the 16 mm distance set of antennas a slightly lower field strength is used, but again here a peak pointing downwards in the middle for the larger field strength can be seen, another one at the right end of the graph is also visible. Besides the two features where one is present inside the electromagnet and with the larger field and one only for the larger field the graphs lay on top of each better than before. Comparing all four graphs of this set of microstrip antennas shows that the graph outside the electromagnet is a bit different than the others here. Maybe it can be attributed to external influences in the environment.

Figure 4.6 shows the comparison of all three sets of microstrip antennas with a YIG waveguide. One unexpected observation is that the peak for the 4 mm distance set of microstrip antennas is in a different frequency range than for the other two. This should not be the case as the position is independent of distance between the antennas. Maybe it could be caused by standing electromagnetic waves between the antennas. As the range is the same for figure 4.3 it could also be that the field strength is set to something different than noted during the experiments. The peak is also more broader and pronounced than for the other sets of antennas. That the blue and orange graphs do not overlap left and right of the peak is also not expected. For the 10 mm distance set the blue graph is a bit lower than the orange one for the right side of the peak. Here the transmission is rather low left and right and more noisy than before which can be attributed to the larger distance. For the 16 mm distance set of antennas the result is more chaotic. A peak is visible for the measurement with a YIG waveguide, but besides that the graphs do not overlap and have a more chaotic progress. Again here the capacitor-like ground can be the cause. However as there is only one set with this ground and the distance between the antennas increases it is not sure if the change can be attributed to the distance or the ground.

In general for the measurement and for the discussion in the section before measurement errors can never be ruled out. A wrong external field strength can be entered for the

electromagnet which could explain shifts in the peaks for the measurements with YIG. Additionally the sets of microstrip antennas are fragile and they could break because of bending. Maybe the sets were bend too much at some point which could have distorted the measurements. Furthermore when changing the measurement setup a short time has to pass for the VNA to sweep over the whole frequency range again and display the new results. It could have happened that the results were saved too early with a mixture of new and old data.

5.3 Comparison of the simulation and the experimental results

For the comparison of the simulation and experimental results for the 4 mm distance set of microstrip antennas in figure 4.7 it can be seen for the S_{11} parameter that both simulations show the ideal case where there is no reflection at all while for the experiment this is not perfectly the case, decreasing with increasing frequency. However the graph goes down to -2.0 dB which is still a sufficient value. For both simulations there is one runaway value, but it coincides with a peak for the S_{21} parameter. For the transmission the simulation data definitely displays more features for both simulations where they show the same resonance peaks while this is not the case for the experimental data. However the experimental and simulation result lay rather close to each other and no other deviations are present. Also both simulations lay on top of each other with just some small differences for small frequencies and for some peak strengths.

This is partly the case for the comparison of the 10 mm distance set of microstrip antennas in figure 4.8. The S_{11} parameter decreases for the measurements and the simulation shows the ideal case, again with the same peak present. For the S_{21} parameter a stronger deviation can be seen as both simulations result in larger values than the experiment and the features cannot be reproduced. The larger difference can be due to more loss in the experiment which is not produced in the simplified case of the simulation. Again the simulations overlap, but they do not fit to the features in the experimental results which is partly distorted by the peaks.

As already explained while introducing the simulation some simplifications are made in the model like the PEC boundary condition which can influence the results and be the cause of deviations and the resonances. Furthermore the built-in values for material properties are only integers and not the most exact ones which influences the behaviour of the whole setup.

Regarding the peaks three out of four resulting length scales are the same for both sets of microstrip antennas. The only thing changing between the two models in the simulation is the distance between the two antennas and with that the curvature between the top and bottom part of the single antennas. The length and width of the straight parts are the same. As the lengths in this direction perpendicular to the distance stay constant and the length scales computed are mostly the same, then it can be assumed that

5 Discussion

the lengths causing the resonances are along this direction following the single microstrip antenna.

The length scales present in both antennas are 10.90 mm, 7.935 mm and 5.761 mm. The last length scale of (5.761 ± 0.037) mm can be attributed to the length scale of the bottom straight part of the antenna of 6.387 mm (see table 3.1). The values are a bit apart and the length is outside of the uncertainty of the calculated value. However as it only serves as a lower boundary it can be assigned to the larger dimension.

Taking the value of (7.935 ± 0.070) mm and dividing it by 3 results in (2.645 ± 0.024) mm which could correspond to the length of the top straight part of the antenna. So here a resonance of $n \cdot \lambda$ with $n = 3$ would happen. Additionally taking the (10.90 ± 0.14) mm and dividing it by 4 gives (2.725 ± 0.033) mm which would result in $4 \cdot \lambda$. This could again be assigned to the same length scale. As both are a bit smaller and only lower bounds it is a bit difficult to determine exactly which length scale would belong to which length in the model. For example the smaller of the two could cause a resonance in the top straight part of the antenna and the larger could cause one in the straight part plus the circular real direct ground with a specific diameter which would have a total value of 3.107 mm. Or they could maybe both cause resonances in the same length scale next to each other. The two additional lengths are (20.56 ± 0.47) mm for the 4 mm distance set of microstrip antennas and (14.59 ± 0.24) mm for the 10 mm distance set of microstrip antennas. The first one could be a multiple of the (2.725 ± 0.033) mm with $n = 8$ and the second one could correspond to the (2.645 ± 0.024) mm with $n = 6$. So the (20.56 ± 0.47) mm and (10.90 ± 0.14) mm are overtones belonging together and the (14.59 ± 0.24) mm and (7.935 ± 0.070) mm do. Even though simple division by integers would not yield the exact results and they lie outside their respective uncertainty this could be correct as all values are again only lower bounds and it is difficult to quantify how large the difference is as the width changes along the single antenna and with that ϵ_e changes.

6 Conclusion

The aim of this thesis is to determine the performance of microstrip antennas and to describe the behaviour of the electromagnetic leakage between the antennas. For this experiments are conducted in different settings and these are compared among each other. Additionally simulations are carried out similar to one type of measurement and the performance of the simulation and the experiments are put side to side.

For the experiments the three microstrip antennas, 4 mm and 10 mm distance with real direct ground and 16 mm distance with capacitor-like ground, were measured in different setups. All were measured outside and inside an electromagnet in the backward volume geometry without an external field where there was no significant difference in the transmitted signal. The set microstrip antennas mentioned first is also measured inside the electromagnet without an external field in two additional geometries, namely forward volume and surface geometry. Again no significant change is visible when compared to the measurement outside the magnet. This set of microstrip antennas is also measured with two different field strengths in all three geometries and the results are compared against each other. Again no visible deviations between them can be made out. In some measurements peaks are visible. An attempt for an explanation is given here, but it is also shown for example for some peaks that they can be smoothed out and do not change the general overlap. Additionally measurements with a YIG waveguide are conducted for BVMSW and MSSW and the peak caused by this is clearly visible. When comparing with the measurement without the YIG a slight difference in transmission is visible which should not be the case. Possible explanations are discussed, but no answer can be given for sure. The measurements are also conducted with the other two sets of antennas, but only in backward volume geometry and for BVMSW. For outside and inside the magnet without an external field a slightly worse result is presented for larger distances between the antennas as the transmission signal gets weak and more features are present. It also holds for the comparison of the measurements with the two different field strengths. Again peaks are visible. The measurements with and without the YIG waveguide are compared and for the 10 mm distance set of microstrip antennas the transmission is more noisy and does overlap better because of this. For the largest distance between the antennas strong fluctuations are present and the overlap is not very good. The center of the peak is different for the smallest distance set in comparison to the other two. That should not be the case and could be caused by measurement errors.

The simulations are carried out for the two sets of microstrip antennas with real direct ground and the transmission and reflection are set side by side with the measurements outside the electromagnet. The results lie close to each other. However the simulation is done with some simplifications which makes comparison of the two more inaccurate.

6 Conclusion

What also leads to deviations are peaks caused by resonances in the simulation data. These peaks are determined and their respective length scales are calculated. For them lengths in the model are assigned which could be the causes for the resonances. For both sets of microstrip antennas almost the same peaks are present.

In general the 4 mm distance set of microstrip antennas proved to be the one with less noise and features and thus a better overlap with the other measurements and with the simulation regardless of the resonance peaks is visible. The shift in position of the peak caused by the YIG waveguide cannot be explained, but further measurements and investigation are needed. Then also the peaks visible in some measurements could be studied in more detail.

Bibliography

- [1] C. Abert. Micromagnetics and spintronics: models and numerical methods. *The European Physical Journal B* 92, 120, 2019.
- [2] J. D. Adam. Analog signal processing with microwave magnetics. *Proceedings of the IEEE* 76, 2, 1988.
- [3] J. D. Adam, J. M. Owens, and J. H. Collins. Studies of FMR in thick YIG films grown by liquid phase epitaxy. *AIP Conf. Proc* 18, 1279, 1974.
- [4] A. V. Chumak, P. Kabos, M. Wu, C. Abert, C. Adelman, A. Adeyeye, J. Åkerman, F. G. Aliev, A. Anane, A. Awad, C. H. Back, A. Barman, G. E. W. Bauer, M. Becherer, E. N. Beginin, V. A. S. V. Bittencourt, Y. M. Blanter, P. Bortolotti, I. Boventer, D. A. Bozhko, S. A. Bunyaev, J. J. Carmiggelt, R. R. Cheenikundil, F. Ciubotaru, S. Cotofana, G. Csaba, O. V. Dobrovolskiy, C. Dubs, M. Elyasi, K. G. Fripp, H. Fulara, I. A. Golovchanskiy, C. Gonzalez-Ballester, P. Graczyk, D. Grundler, P. Gruszecki, G. Gubbiotti, K. Guslienko, A. Haldar, S. Hamdioui, R. Hertel, B. Hillebrands, T. Hioki, A. Houshang, C. M. Hu, H. Huebl, M. Huth, E. Iacocca, M. B. Jungfleisch, G. N. Kakazei, A. Khitun, R. Khymyn, T. Kikkawa, M. Kläui, O. Klein, J. W. Kłos, S. Knauer, S. Koraltan, M. Kostylev, M. Krawczyk, I. N. Krivorotov, V. V. Kruglyak, D. Lachance-Quirion, S. Ladak, R. Lebrun, Y. Li, M. Lindner, R. Macêdo, S. Mayr, G. A. Melkov, S. Mieszczak, Y. Nakamura, H. T. Nembach, A. A. Nikitin, S. A. Nikitov, V. Novosad, J. A. Otalora, Y. Otani, A. Papp, B. Pigeau, P. Pirro, W. Porod, F. Porrati, H. Qin, B. Rana, T. Reimann, F. Riente, O. Romero-Isart, A. Ross, A. V. Sadovnikov, A. R. Safin, E. Saitoh, G. Schmidt, H. Schultheiss, K. Schultheiss, A. A. Serga, S. Sharma, J. M. Shaw, D. Suess, O. Surzhenko, K. Szulc, T. Taniguchi, M. Urbánek, K. Usami, A. B. Ustinov, T. van der Sar, S. van Dijken, V. I. Vasyuchka, R. Verba, S. V. Kusminskiy, Q. Wang, M. Weides, M. Weiler, S. Wintz, S. P. Wolski, and X. Zhang. Roadmap on spin-wave computing, 2021.
- [5] COMSOL. Eigenfrequency. visited on July 12th, 2023.
- [6] COMSOL. Frequency domain. visited on July 12th, 2023.
- [7] COMSOL. Frequency domain, modal. visited on July 12th, 2023.
- [8] COMSOL. Physics-controlled meshing. visited on July 11th, 2023.
- [9] COMSOL. RF module, user's guide. Version COMSOL 5.4.

Bibliography

- [10] W. Frei. Modeling metallic objects in wave electromagnetics problems. visited on July 12th, 2023.
- [11] H. Johnson and M. Graham. *High-Speed Signal Propagation*. Prentice Hall Professional Technical Reference, 2003.
- [12] K. M. Krishnan. *Fundamentals and applications of magnetic materials*. Oxford university press, 2016.
- [13] B. M. Lebed, S. V. Yakovlev, S. J. Gavrilko, V. A. Dubovoy, A. V. Nikiforov, and H. S. Rutstein. Microwave devices based on magnetostatic surface waves propagated in thin magnetic films. *Microwave Journal* 38, 5, 1995.
- [14] P. Matthews. Filter basics part 3: Five key filter specifications to understand. visited on August 30th, 2023.
- [15] L. Miller. *RF Filter Technologies For Dummies*. John Wiley & Sons, Inc., 2015.
- [16] D. M. Pozar. *Microwave engineering: fourth edition*. John Wiley & Sons, Inc., 2012.
- [17] A. Savitzky and M. J. E. Golay. Smoothing and differentiation of data by simplified least squares procedures. *Analytical Chemistry*, 36:1627–1639, Jan. 1964.
- [18] A. A. Serga, A. V. Chumak, and B. Hillebrands. Yig magnonics. *Journal of Physics D: Applied Physics*, 43(26):264002, jun 2010.
- [19] N. Zenbaa. Propagating Spin Wave Spectroscopy (PSWS) in micrometer-thick magnetic layers, 2022.

Acronyms

BVMSW backward volume magnetostatic spin waves. 14, 21, 22, 30, 35

FVMSW forward volume magnetostatic spin waves. 14

GGG Gadolinium Gallium garnet. 1, 11, 15, 16, 31

LLG Landau-Lifshitz-Gilbert. vii, 3, 5–7

MSSW magnetostatic surface spin waves. 1, 14, 21, 30, 31, 35

MSW magnetostatic waves. vii, 1, 2, 14, 21

PEC perfect electric conductor. 16, 33

S-Parameter scattering parameter. i, 11, 12, 14, 16, 21

VNA vector network analyzer. i, vii, 11, 12, 14, 29, 33

YIG Yttrium Iron garnet. i, vii, viii, 1, 2, 11, 14, 20–24, 30–33, 35, 36